Environ. Sci. Technol. **2006**, *40,* 5010−5014

Localizing the Biochemical Transformations of Arsenate in a Hyperaccumulating Fern

INGRID J. PICKERING,*,† LUKE GUMAELIUS,‡,§ HUGH H. HARRIS,∥ ROGER C. PRINCE,# GREGORY HIRSCH,⊥ JO ANN BANKS,‡ DAVID E. SALT,§ AND GRAHAM N. GEORGE*,†

Department of Geological Sciences, University of Saskatchewan, 114 Science Place, Saskatoon, Saskatchewan S7N 5E2, Canada, Departments of Botany, Plant Pathology, and Horticulture and Landscape Architecture, Purdue University, West Lafayette, Indiana 47907, School of Chemistry, University of Sydney, New South Wales 2006, Australia, ExxonMobil Biomedical Sciences Incorporated, Annandale, New Jersey 08801, and Hirsch Scientific, Pacifica, California 94044

The fern *Pteris vittata* accumulates unusually high levels of arsenic. Using X-ray absorption spectroscopy (XAS) and XAS imaging, we reveal the distribution of arsenic species in vivo. Arsenate is transported through the vascular tissue from the roots to the fronds (leaves), where it is reduced to arsenite and stored at high concentrations. Arsenic-thiolate species surrounding veins may be intermediates in this reduction. In gametophytes, arsenite is compartmentalized within the cell vacuole. Arsenic is excluded from cell walls, rhizoids, and reproductive areas. This study provides important insights into arsenic hyperaccumulation, which may prove useful for phytoremediating arsenic-contaminated sites, and demonstrates the strengths of XAS imaging for distinguishing highly localized species.

Introduction

The Chinese or ladder break fern *Pteris vittata* (*1*), and a few of its relatives (*2*), are the only known hyperaccumulators of arsenic—plants that both accumulate and tolerate highly magnified levels of this metalloid their shoots (*3*). Arsenic is well-known for its toxicity, being variously a metabolic and respiratory inhibitor, depending upon its chemical form (*4*). The discovery that *P. vittata* actively concentrates and tolerates high levels of arsenic thus lead to widespread interest. Even more remarkable is the fact that *P. vittata* converts the less toxic arsenate present in the soil to the much more deadly arsenite (*5*, *6*). Here we present an in situ X-ray absorption spectroscopy (XAS) and XAS imaging study to provide insights into how *P. vittata* copes with its deadly cargo. We examine living tissues both of the diploid sporophyte, the dominant, spore-forming phase of the fern life cycle with the more complex and familiar leafy form, and of the haploid gametophyte, also free-living and photosynthetic, but small (2−3 mm) and mostly one cell thick (*7*). The examination of both phases of the fern life cycle provides a unique opportunity to study arsenic hyperaccumulation at the organ, tissue, and cellular levels.

Materials and Methods

Specimen Origin. A mature sporophyte fern collected in proximity to a chromated copper arsenate wood treatment facility at site 11 as described by Gumaelius et al. (*8*) was imaged 3 weeks after collection. Prior to imaging the still viable sporophyte had been cultivated, without additional arsenic amendment in its native soil, at a Purdue University greenhouse.

Gametophyte and Sporophyte Cultivation. Spores collected from field-collected sporophytes (*8*) were sterilized (*9*) and grown either in 1/2 strength Murashige and Skoog pH 6.5 liquid media shake cultures amended with 1 mM potassium arsenate (KH_2AsO_4) or solid-surface agar culture of the same composition. In both cases, cultures were grown at 26 °C under 24 h fluorescent lighting. One-month-old gametophytes from both culture methods were examined using X-ray absorption spectroscopy (XAS). Four-month-old sporophytes grown under 24 h fluorescent lighting at 26 °C on rock-wool saturated with 1/2 strength Murashige and Skoog liquid media amended with 1 mM KH_2AsO_4 were also examined with XAS.

X-ray Absorption Spectroscopy. Arsenic K-edge X-ray absorption spectroscopy (XAS) was carried out at the Stanford Synchrotron Radiation Laboratory (SSRL), with the SPEAR storage ring operating at 80−100 mA. Beamlines 7−3 and 9−3 were used, each equipped with a Si(220) double crystal monochromator. Beamline 7−3 had a premonochromator aperture of 1 mm with no focusing optics, and harmonic rejection was achieved by detuning one of the monochromator crystals to give 50% of the peak intensity. Beamline 9−3 had an upstream collimating mirror and a downstream sagittally focusing mirror; both were Rh-coated and also provided harmonic rejection. Incident and transmitted intensities were measured with nitrogen-filled ion chambers. Bulk samples were maintained at ∼10 K in a liquid helium flow cryostat and positioned at 45° to the incident beam. Spectra were measured by monitoring the As K_α fluorescence using a Canberra 30-element germanium detector (*10*) at 90° to the incident beam, taking care to maintain the count-rates within the pseudolinear regime. Energies were calibrated with respect to the spectrum of elemental α-arsenic, collected in transmittance simultaneously with that of the sample, the first energy inflection of which was assumed to be 11 867.0 eV.

Quantitative analysis of near-edge spectra were carried out by least-squares fitting of spectra of standard compounds (Figure 1A−E) to the spectra of the fern tissues, according to established procedures (*11*, *12*). The errors are obtained as precisions and are given as three times the estimated standard deviation obtained from the diagonal elements of the covariance matrix. The fractional contribution of the near-edge of a standard to the fit is then equivalent to the fractional abundance of that arsenic standard in the sample.

XAS Imaging. XAS imaging used the method previously described by Pickering et al. for selenium (*13*). Data were collected at beamline 9−3 at SSRL, where microfocus X-ray beams of 15 or 5 μm diameter were provided by tapered

* Corresponding author phone: +01-306-966-5706 (I.J.P.) and +01-306-966-5722 (G.N.G.); e-mail: Ingrid.pickering@usask.ca (I.J.P.) and g.george@usask.ca (G.N.G.).
† University of Saskatchewan.
‡ Department of Botany, Purdue University.
§ Departments of Plant Pathology and Horticulture and Landscape Architecture, Purdue University.
∥ University of Sydney.
ExxonMobil Biomedical Sciences Inc.
⊥ Hirsch Scientific.

10.1021/es052559a CCC: $33.50
Published on Web 07/12/2006

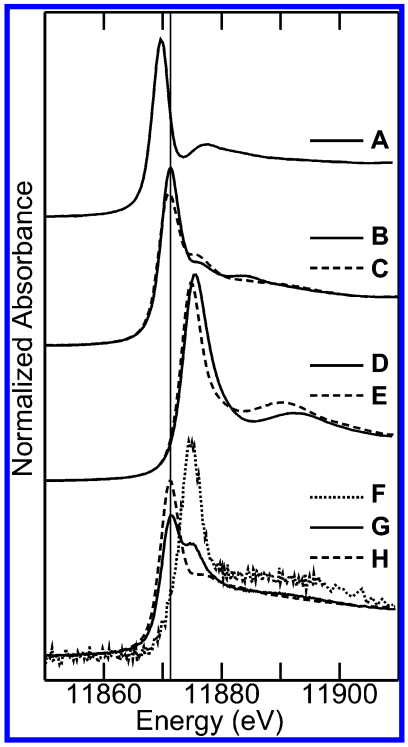

FIGURE 1. Arsenic K near-edge spectra of aqueous solutions of standards and *P. vittata* sporophyte tissues. As^{III} tris-glutathione [$As(SR)_3$] (A); arsenite at pH 7.0 (B) and 10.5 (C); arsenate at pH 4.5 (D) and 9.0 (E); *P. vittata* rhizoids (F), stems (G), and pinnae (H).

metal monocapillaries (*14*, *15*). The beamline energy was recalibrated before each measurement with reference to an arsenic metal foil (as described above). Each tissue sample was mounted at room temperature in a humid environment and placed normal to the microbeam and ~100 μm from the monocapillary exit aperture. Arsenic K_α fluorescence and scattered intensities were monitored using a single element Ge detector and transmitted intensities using a nitrogen-filled ion chamber. The sample was spatially rastered in the microbeam using a Newport PM500 stage. Energies for the chemically specific imaging were chosen with reference to standard spectra of aqueous solutions collected under identical conditions; the energies corresponded to the peak absorption of the standards which were 11 869.8, 11 871.4, and 11 874.8 eV for As(glutathione)$_3$, arsenite, and arsenate, respectively. A horizontal raster was collected at each energy, before changing the vertical position, thus ensuring that data were collected on a given pixel in the shortest amount of time (*15*). Windowed fluorescence data were corrected for scatter as previously described (*13*). Quantities of arsenic per pixel were calibrated by recording the fluorescence intensities from a standard solution of arsenic (5 mM aqueous arsenate) of a known path length (2 mm). Concentrations were then derived from the arsenic quantities together with the transmittance maps, assuming density and X-ray absorption cross-section of water, as previously described (*13*).

Results and Discussion

We have employed bulk XAS to assess which arsenic species are present and XAS imaging to determine their spatial localization. Both were applied to fresh, living tissues essentially without pretreatment. The sensitivity of arsenic XAS to chemical type and pH is illustrated in Figure 1A−E, which shows near-edge spectra of aqueous solutions of arsenate, arsenite, and thiolate-coordinated As^{III} [$As(SR)_3$] (*12*). The bulk sporophyte near-edge spectra (Figure 1F−H) were quantitatively analyzed by fitting to the sum of aqueous

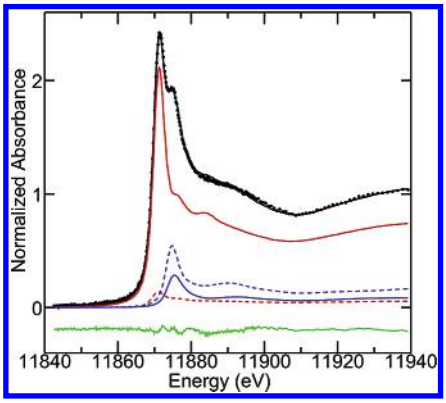

FIGURE 2. Quantitative analysis of the stem As near-edge spectrum by fitting to the sum of aqueous standard spectra. The figure shows the data as small circles, best fit as the overlayed solid black line, and the residual as the solid green line offset below. Components of the fit are shown as follows: 70.2 ± 1.4% aqueous arsenite at pH 7.0 (solid, red), 5.3 ± 1.5% aqueous arsenite at pH 10.5 (dashed, red), 8.2 ± 0.5% arsenate pH 4.5 (solid, blue), 16.3 ± 0.6% arsenate pH 9.0 (dashed, blue). Using literature pK_a values this yields values of pH of approximately 8.1 and 7.3 for arsenite and arsenate, respectively. Errors are estimated to be 0.5 and 0.2 pH units, respectively. The errors are larger for the more abundant arsenite because of the similarity in the spectra of its two pH forms.

standard spectra (an example of this is shown in Figure 2 for the stem). The root spectrum, noisy due to very low arsenic concentration, contained predominantly arsenate (90 ± 4%), with a minor component of arsenite (10 ± 5%). The rachis (the midrib of the fern blade) showed a mixture of 24% arsenate at pH 7.3 and 76% arsenite at pH 8.1, with no significant $As(SR)_3$ (Figure 2). The leaves showed predominantly arsenite (95 ± 1%) at near-neutral pH with a trace (5 ± 1%) of $As(SR)_3$ and, in agreement with previous work (*5*), the highest arsenic levels. In contrast, arsenate-treated *Brassica juncea* showed reduction to $As(SR)_3$ and storage in the roots (*12*). However, *B. juncea* did show low concentrations of arsenate and arsenite in the xylem exudates (*12*), similar to the speciation of *P. vittata* rachis tissue.

Having identified the compounds present, we used XAS imaging to determine their localizations *in planta*. The energy of a microfocused X-ray beam is tuned to the peak spectral absorption for each chemical species, and the fluorescence and absorption intensities are measured as the sample is raster scanned. Deconvolution yields the concentrations of the individual chemical species (*13*). XAS images are shown in Figure 3 for the tip of a pinna (one element of the compound leaf), a portion of a rachis (the midrib of the fern blade), and spore-forming sporangia (small purse-shaped structures with enclosed spores), of a sporophyte grown in arsenate-laden soil.

The pinna tip (Figure 3A−D) is dominated by arsenite (Figure 3C). Arsenite concentration is highest (up to 25 mM) in the blade proximal to the veins, falling off with distance and is lowest within the veins themselves. In contrast, arsenate shows very low concentrations within the blade tissue but is localized within the veins at up to 1 mM. Its maximum concentration is only ~5% of that of arsenite, and since it is localized in very narrow structures, it is not surprising that it was not detected in the bulk spectra of leaves.

The rachis shows arsenate (Figure 3H) confined to the central 40% of the mid-vein and stem in bundles of parallel strands, some individually <40 μm across. The bundles, ~170 μm across in the mid-vein and double that in the rachis, correspond to the location of the transport vessels. The arsenite image (Figure 3G) is dominated by high leaf blade concentrations, while the rachis and mid-vein show much

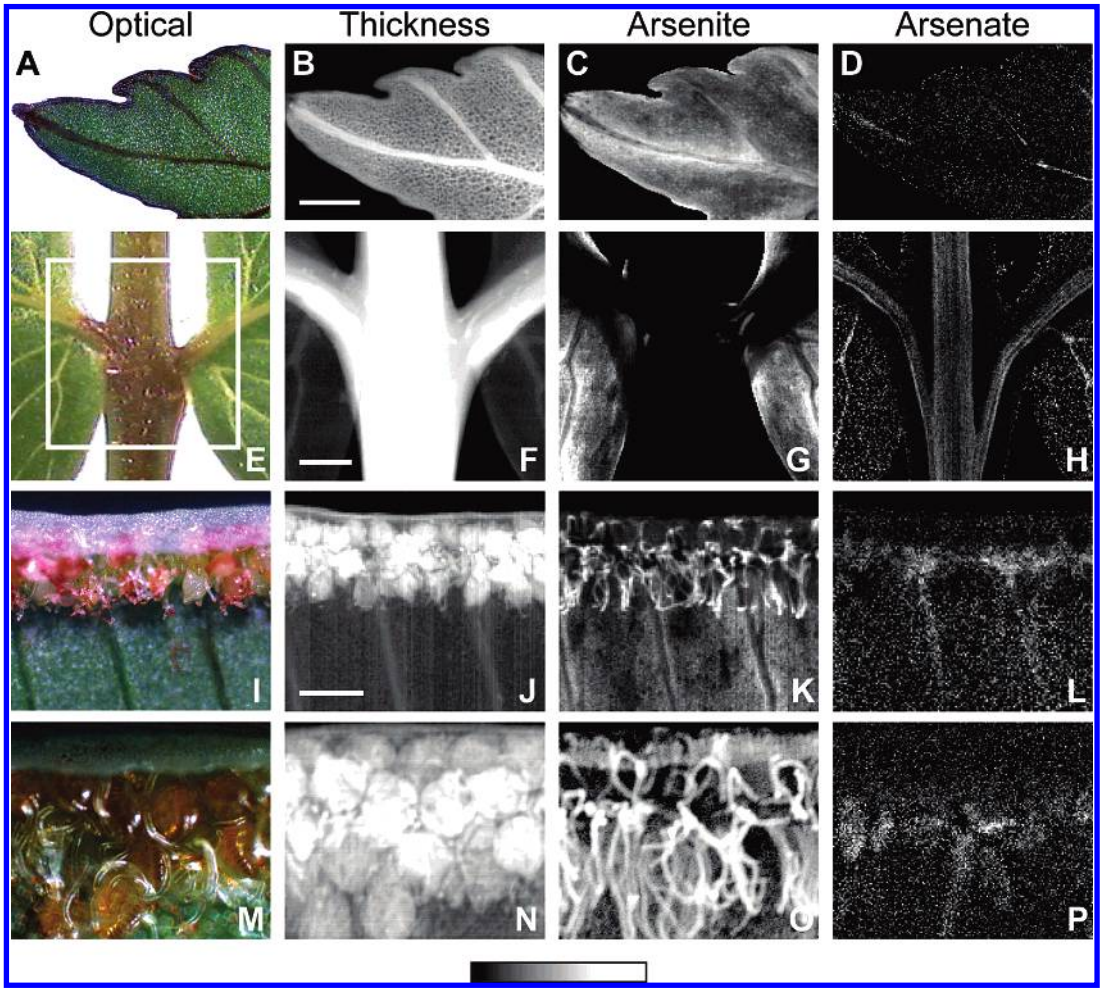

FIGURE 3. Arsenic K-edge XAS images of *P. vittata* sporophyte tissues. Tip of pinna (leaf) (A−D), rachis (E−H), and two views of the regions of sporangial growth at pinnal edges (I−P), each showing optical micrograph, thickness, and the concentration of arsenite and arsenate. Scalebars are 500 μm; step sizes are 10 μm (B−D), 15 μm (F−H, J−L), and 6 μm (N−P). Maxima are B: 0.2 mm, C: 40 μM, D: 2 μM, F: 1.3 mm, G: 20 μM, H: 2 μM, J: 0.9 mm, K: 25 μM, L: 2 μM for N−P the intensity scales are arbitrary. In N−P the images are magnified by a factor of 2.2 relative to J−L.

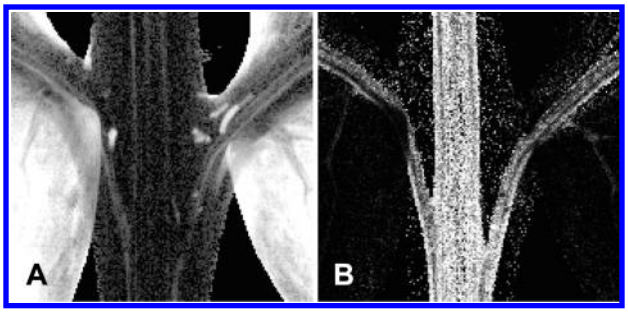

FIGURE 4. XAS images of *P. vittata* stem from Figure 3E−H. Arsenite, log (concentration [mM]), scaled −4 to +2 to emphasize transport vessels (A). Fraction of arsenic as arsenate (scaled 0 to 1) (B). The lower intensity streaks within the bundles of (B) correspond to arsenite.

lower arsenite concentrations. However, close examination (see Figure 4) reveals strands of arsenite interleaved (but not coincident) with those of arsenate. We hypothesize that the arsenate and arsenite strands may be the xylem and phloem, respectively. The recent finding that xylem exudates contain arsenate (*16*) is in agreement with this. When the sporophyte from Figure 3 was imaged some 2 months later (not illustrated) having been given only water (i.e. no arsenic), the arsenate in the central structures was substantially diminished. We conclude that this was due to depletion of arsenate in the original soil by incorporation into the tissues and growth of the plant. XAS imaging on plants grown entirely in the laboratory on rock wool with arsenate in their growth media showed essentially identical arsenic localization to that shown in Figures 3 and 4 (not illustrated).

The sporangia (Figure 3I−L) show arsenate at low concentrations within the veins (including under the sporangia, Figure 3L,P), while arsenite is present at locally high concentrations close to the sporangia. A higher-resolution scan (Figure 3M−P) resolves the spores in the transmittance (thickness) image, ∼50−70 μm across inside the pouchlike sporangia (∼200−250 μm across). In contrast to previous reports (*17*), arsenite is excluded from the spores and sporangia but is preferentially concentrated within the paraphyses, sterile hairlike structures adjacent but not directly associated with the sporangia (Figure 3O). Arsenite also accumulates within the pseudoindusium, the reflexed margin of the lamina that partially covers the sporangia (Figure 3O).

Pteris vittata gametophytes also hyperaccumulate arsenic (*8*), and Figure 5 shows XAS images for three gametophytes. They contain predominantly arsenite, localized within the center of the cells and absent from the cell walls. This is consistent with arsenite storage within the cellular vacuole, which in fully expanded fern cells is typically large, centrally located, and dominates the cell volume. However, specific regions of the gametophyte reproducibly show no significant arsenite: specifically cell walls, rhizoids (slender rootlike filaments through which nourishment is absorbed), and the

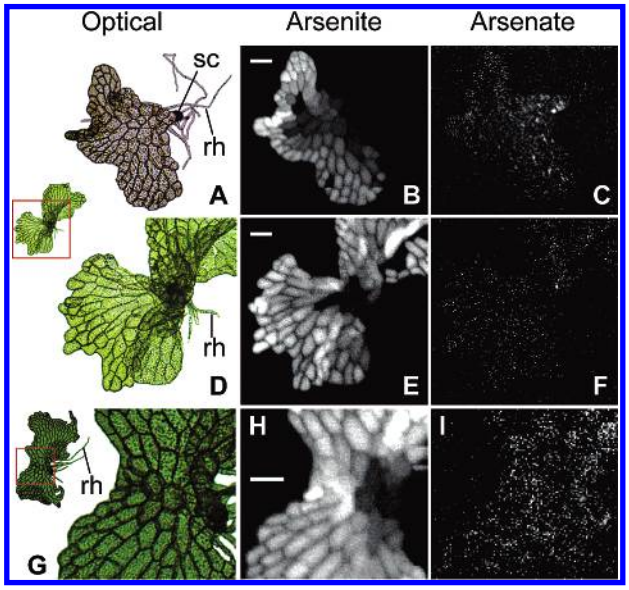

FIGURE 5. XAS images of *P. vittata* gametophytes grown in shake culture, showing optical micrographs (A, D, G), arsenite amounts (B, E, H), and arsenate amounts (C, F, I). Scalebars are 100 μm; step size is 5 μm (6 μm for H, I). Maximum intensities for B, E, and H are 0.8, 0.8, and 0.5 μmol·cm^{-2}, respectively. Arsenate image intensities are ~10% those of corresponding arsenite images, zero offset for clarity. rh indicates the rhizoids, and sc the spore coat. Note that the thickness is in this case unavailable as the samples were measured in a thin film of water to prevent dehydration.

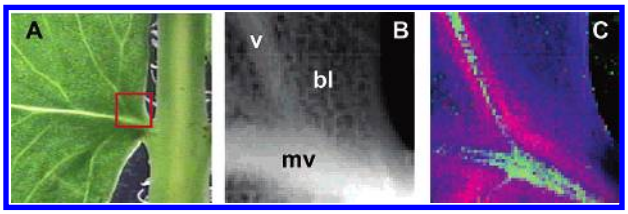

FIGURE 6. Three-component XAS imaging of *P. vittata* leaf. Optical micrograph (A), thickness (B), RGB image showing concentrations of arsenite (blue), arsenate (green), and As(SR)$_3$ (red). (C). mv indicates midvein, v a vein, and bl the leaf blade.

regions from which the rhizoids arise. Overall, gametophyte arsenate content is very low but appears to be localized as speckles ~10 μm across distributed throughout the gametophyte cells, including those in which arsenite is not present (Figure 5C,F,I). The nature of the arsenate speckles is unknown, but they may be Golgi bodies or other specialized structures that take up and store arsenate prior to reduction and vacuolar storage.

A surprising aspect of the fern's hyperaccumulation of arsenic is the apparent low involvement of thiolate coordination, despite the high affinity of As^{III} for sulfur ligands and the typically large intracellular abundance of thiols (*18*). Our bulk XAS spectroscopy (Figure 1H) confirms that the preponderance of arsenic is coordinated by oxygen, rather than thiolates (*5*). We find marginal contributions of thiolates both in the edge (Figure 1H) and extended X-ray absorption fine structure (EXAFS) (not shown) of leaf tissues, though not in the stems or gametophytes. To determine the localization of this thiolate-coordinated arsenic, three-component XAS images were recorded on the leaves of *P. vittata* sporophytes grown on rockwool irrigated with 1 mM arsenate solution (Figure 6). These images clearly reveal highly localized thiolate-coordination in close proximity to the vein and mid-vein. The center of the vein shows arsenate, ~35 μm across (Figure 6C), while the thiolates appear as a cylindrical sheath, 40−50 μm thick, immediately surrounding the arsenate (Figure 6C). μ-X-ray absorption near-edge spectra collected from regions showing the highest proportions of arsenite, arsenate, and As(SR)$_3$, confirmed the localization shown by the XAS imaging results.

The presence of the arsenic-thiolates appears to be linked to the presence of arsenate in the vein. Similar images of a sporophyte that had depleted the original arsenate from its soil revealed high concentrations of arsenite in the leaf blade but neither arsenate nor thiolates. This strongly suggests that thiolates appear in response to actively transported arsenate, and their presence in a cylindrical sheath around the vein suggests a single layer of cells with a special purpose. Webb et al. (*5*) also found small thiolate contributions in both edge and EXAFS spectra of thawed sporophytes, although this might have been due to chemical reactions of cellular contents after cell breakage following freezing. Additionally, *P. vittata* synthesizes phytochelatins in response to arsenate, although only in amounts sufficient to coordinate ~3% of the total arsenic in the leaves (*19*). Together, these observations indicate that only a small fraction of arsenic in leaves is coordinated to thiolates. This lack of thiol coordination may be a common theme in plants that have evolved to hyperaccumulate metals, including Ni (*20*), Zn (*21*), Cd (*22*), Se (*13*), and As, compared to the involvement of thiols in nonadapted plants to coordinate Cd (*23*) and As (*12*).

Our demonstration that *P. vittata* transports arsenate to the frond's photosynthetic tissues are in apparent contradiction to the EXAFS (not near-edge spectra) of Huang et al. (*24*) that detected only arsenite in *P. vittata*, including the roots. Given the low levels of arsenic in the roots, minor contamination with leaf tissue could explain this discrepancy. The work reported by Duan et al. (*25*) measuring glutathione-dependent arsenate reductase activity only in the roots is also in apparent conflict with our conclusions. Glutathione-dependent arsenate reductases are well-known in yeast (*26*), and a number of other arsenate reductases have been characterized, including mammalian (*27*) and bacterial (*28*) forms that are unrelated to the yeast enzymes. To date, there is no evidence tying the in vitro arsenate-stimulated glutathione-dependent reductase activity in *P. vittata* roots (*25*) with the in vivo process we have observed. Identifying *P. vittata*'s arsenate reductase awaits genetic and other evidence.

Our work demonstrates the strength of XAS imaging at multiple wavelengths, rather than microspectroscopy at select pixels, to determine chemical form. The arsenate is present in such low concentrations compared with the arsenite that details of the transport vessels and gametophyte cells would have been completely obscured using single-energy microprobe. Additionally, the acquisition of spectra at such low concentrations would necessitate data collection for several minutes, possibly with significant sample degradation and ablation. By contrast, in XAS imaging the sample is only illuminated for less than a second per pixel, causing considerably less damage to the sample. Likewise, the localization of the thiolates in the sporophyte would have remained obscure without this method.

Our experiments, directly visualizing arsenic forms in intact fern tissues, provide compelling evidence that *P. vittata* transports untransformed arsenate to the frond. Arsenic is largely excluded from the stems and is predominantly stored within the leaf tissues as neutral arsenite. Thiolates appear as a cylinder around the arsenate in the veins and may be part of the reduction pathway. Arsenate is seen in the veins supporting the sporangia but is excluded from the sporangia and spores themselves. When transformed to arsenite, it is localized to the paraphyses surrounding the sporangia (paraphyses are sterile hairs intermixed with the sporangia, believed to perform a protective fuction). Gametophytes clearly show arsenite uniformly localized within the vacuole

of fully expanded cells but excluded from specific regions of the gametophyte, including the rhizoids' egg-forming archegonia. Discrete speckles of arsenate are localized in unknown subcellular compartments. Future work at higher resolution will investigate the subcellular localization of these species and attempt to further elucidate the biochemistry of hyperaccumulation for this most interesting fern.

Acknowledgments

This work was carried out in part at the Stanford Synchrotron Radiation Laboratory which is funded by the U.S. Department of Energy, Offices of Basic Energy Sciences and Biological and Environmental Research, and by the U.S. National Institutes of Health, National Center for Research Resources BMTP. I.J.P. and G.N.G. acknowledge support from Canada Research Chair awards, the Province of Saskatchewan, the University of Saskatchewan, the Natural Sciences and Engineering Research Council (Canada), and the Canadian Institutes for Health Research. We thank Dr. Satya P. Singh, Dr. Christian J. Doonan, and Ms. Limei Zhang (all of the University of Saskatchewan) for assistance with data acquisition. J.B. and D.E.S. acknowledge support from the DOE (DE-FG02-03ER63622). H.H.H. was supported by an Australian Synchrotron Research Program Postdoctoral fellowship and an Australian Research Council Discovery Program grant (DP346162).

Literature Cited

(1) Ma, L Q.; Komar, K M.; Tu, C.; Zhang, W.; Cai, Y.; Kennelley, E. D. A fern that hyperaccumulates arsenic. *Nature* **2001**, *409*, 579.

(2) Meharg, A. Variation in arsenic accumulation − hyperaccumulation in ferns and their allies. *New Phytol.* **2003**, *157*, 25−31.

(3) Kraemer, U. Phytoremediation: novel approaches to cleaning up polluted soils. *Curr. Opin. Biotechnol.* **2005**, *16*, 133−141.

(4) Ord, M. G.; Stockton, L. A. A Contribution to Chemical Defense in World War II. *Trends Biochem. Sci.* **2000**, *25*, 253−256.

(5) Webb, S. M.; Gaillard, J.-F.; Ma, L. Q.; Tu, C. XAS Speciation of Arsenic in a Hyper-Accumulating Fern. *Environ. Sci. Technol.* **2003**, *37*, 754−760.

(6) Tu, C.; Ma, L. Q.; Bondada, B. Arsenic accumulation in the hyperaccumulator Chinese brake and its utilization potential for phytoremediation. *J. Environ. Qual.* **2002**, *31*, 1671−1675.

(7) Raven, P. H.; Evert, R. F.; Eichhorn, S. E. *Biology of Plants*, 5th ed.; Worth: New York.

(8) Gumaelius, L.; Lahner, B.; Salt, D. E.; Banks, J. A. Arsenic hyperaccumulation in gametophytes of *Pteris vittata*. A new model system for analysis of arsenic hyperaccumulation. *Plant Physiol.* **2004**, *136*, 3198−3208.

(9) Banks J. A. Sex-determining genes in the homosporous fern *Ceratopteris*. *Development* **1994**, *120*, 1949−1958.

(10) Cramer, S. P.; Tench, O.; Yocum, M.; George, G. N. A 13-Element Ge Detector for Fluorescence EXAFS. *Nucl. Instrum. Methods Phys. Res., Sect. A* **1988**, *A266*, 586−591.

(11) Pickering, I. J.; Prince, R. C.; Divers, T. C.; George, G. N. Sulfur K-edge X-ray Absorption Spectroscopy for Determining the Chemical Speciation of Sulfur in Biological Systems. *FEBS Lett.* **1998**, *441*, 11−14.

(12) Pickering, I. J.; Prince, R. C.; George, M. J.; Smith, R. D.; George G. N.; Salt, D. E. Reduction and Coordination of Arsenic in Indian Mustard. *Plant Physiol.* **2000**, *122*, 1171−1177.

(13) Pickering, I. J.; Prince, R. C.; Salt, D. E.; George, G. N. Quantitative chemically-specific imaging of selenium transformation in plants. *Proc. Natl. Acad. Sci. U.S.A.* **2000**, *97*, 10717−10722.

(14) Hirsch, G. Metal capillary optics: Novel fabrication methods and characterization. *X-Ray Spectrom.* **2003**, *32*, 229−238.

(15) Pickering, I. J.; Hirsch, G.; Prince, R. C.; Sneeden, E. Y.; Salt, D. E.; George, G. N. Imaging of selenium in plants using tapered metal monocapillary optics. *J. Synchrotron Radiat.* **2003**, *10*, 289−290.

(16) Kertulis, G. M.; Ma, L. Q.; MacDonald, G. E.; Chen, R.; Winefordner, J. D.; Cai, Y. Arsenic speciation and transport in *Pteris vittata* L. and the effects on phosphorus in the xylem sap. *Environ. Exp. Bot.* **2005**, *54*, 239−247.

(17) Lombi, E.; Zhao, F.-J.; Fuhrmann, M.; Ma, L. Q.; McGrath, S. P. Arsenic distribution and speciation in the fronds of the hyperaccumulator *Pteris vittata*. *New Phytol.* **2002**, *156*, 195−203.

(18) Foyer, C. H.; Theodoulou, F. L.; Delrot, S. The functions of inter- and intracellular glutathione transport systems in plants. *Trends Plant Sci.* **2001**, *6*, 486−492.

(19) Zhao, F. J.; Wang, J. R.; Barker, J. H. A.; Schat, H.; Bleeker, P. M.; McGrath, S. P. The role of phytochelatins in arsenic tolerance in the hyperaccumulator *Pteris vittata*. *New Phytol.* **2003**, *159*, 403−410.

(20) Kraemer, U.; Pickering, I. J.; Prince, R. C.; Raskin, I.; Salt, D. E. Subcellular localization and speciation of nickel in hyperaccumulator and non-accumulator *Thlaspi* species. *Plant Physiol.* **2000**, *122*, 1343−1353.

(21) Salt, D. E.; Prince, R. C.; Baker, A. J. M.; Raskin, I.; Pickering, I. J. Zinc Ligands in the Metal Hyperaccumulator *Thlaspi caerulescens* As Determined Using X-ray Absorption Spectroscopy. *Environ. Sci. Technol.* **1999**, *33*, 713−717.

(22) Ebbs, S.; Lau, I.; Ahner, B.; Kochian, L. Phytochelatin synthesis is not responsible for Cd tolerance in the Zn/Cd hyperaccumulator Thlaspi caerulescens (J. & C. Presl). *Planta* **2002**, *214*, 635−640.

(23) Salt, D. E.; Prince, R. C.; Pickering, I. J.; Raskin, I. Mechanisms of cadmium mobility and accumulation in Indian mustard. *Plant Physiol.* **1995**, *109*, 1427−1433.

(24) Huang, Z.; Chen, T.; Lei, M.; Hu, T. Direct determination of arsenic species in arsenic hyperaccumulator *Pteris vittata* by EXAFS. *Acta Bot. Sin.* **2004**, 46, 46−50.

(25) Duan, G.-L.; Zhu, Y.-G.; Tong, Y.-P.; Cai, C.; Kneer, R. Characterization of arsenate reductase in the extract of roots and fronds of Chinese brake fern, an arsenic hyperaccumulator. *Plant Physiol.* **2005**, *138*, 461−469.

(26) Mukhopadhyay, R.; Rosen, B. P. Arsenate reductases in prokaryotes and eukaryotes. *Environ. Health Perspect. Suppl.* **2002**, *110*, 745−748.

(27) Radabaugh, T. R.; Aposhian, H. V. Enzymatic reduction of arsenic compounds in mammalian systems: reduction of arsenate to arsenite by human liver arsenate reductase. *Chem. Res. Toxicol.* **2000**, *13*, 26−30.

(28) Krafft, T.; Macy, J. M. Purification and characterization of the respiratory arsenate reductase of *Chrysiogenes arsenatis*. *Eur. J. Biochem.* **1998**, *255*, 647−653.

Received for review December 21, 2005. Revised manuscript received May 15, 2006. Accepted May 31, 2006.

ES052559A